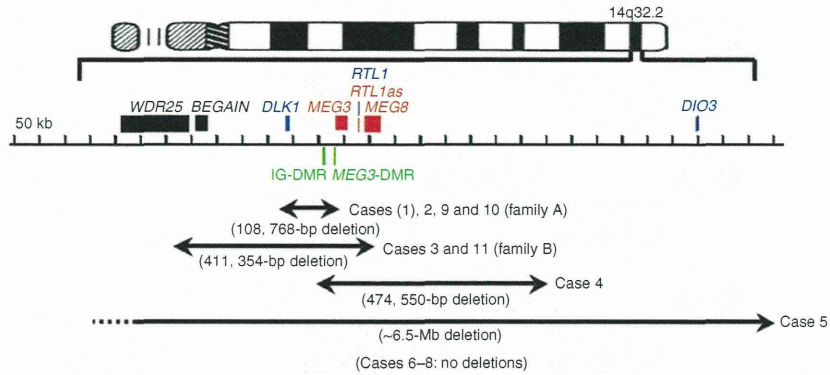

Figure 2 The regional physical map of the human chromosome 14q32.2 imprinted region and the four deletion intervals identified in this study. PEGs are shown in blue and MEGs are shown in red, although it remains to be clarified whether *DIO3* is a PEG; mouse *Dio3* is known to be preferentially but not exclusively expressed from a paternally derived chromosome in embryos[25]. *DAT*[2] (not shown) may also be a PEG in the human, and *Mirg* (*Meg9*)[18] resides between *Rian* (*Meg8*) and *Dio3* in the mouse. *WDR25* and *BEGAIN* seem to be biparentally expressed genes. The two DMRs are depicted in green. The electrochromatograms indicating the fusion points of the three microdeletions are shown in **Supplementary Figure 3**, together with the physical maps representing the deleted regions. The FISH findings identifying the 14q32.2 breakpoint of the r(14) chromosome in case 5 are also shown in **Supplementary Figure 3**. Case 1 of family A was not studied, and no deletion has been identified in cases 6–8.

The human 14q32.2 imprinted region is highly conserved on the distal part of mouse chromosome 12 (ref. 18), in which the germline-derived IG-DMR functions as a *cis*-acting regulator for the imprinted region of maternal origin[4,19]. Targeted deletion of the IG-DMR (ΔIG-DMR) causes paternalization of a maternally derived imprinted region and a unique phenotype comparable to that of paternal uniparental disomy for chromosome 12 (PatDi(12)) in embryos, with ~4.5 times of *Rtl1* expression and ~2 times of *Dlk1* and *Dio3* expression as well as nearly absent expression of MEGs in this imprinted region[4,20,21]. The markedly increased *Rtl1* expression is ascribed to the cumulative effect of the activation of the usually silent maternally derived *Rtl1* and the loss of the microRNA-containing *Rtl1as*, which acts as a repressor for *Rtl1* (refs. 4,9,10). The doubled *Dlk1* and *Dio3* expression is simply a result of the activation of PEGs of maternal origin[4]. The absent MEGs expression is associated with hypermethylation of the *Gtl2*-DMR[4], and this is consistent with the notion that the *Gtl2*-DMR can stay hypomethylated only in the presence of the hypomethylated IG-DMR[4,19]. By contrast, the ΔIG-DMR has no imprinting or clinical effect after paternal transmission[4].

The upd(14)pat-like phenotypes in cases 1–8 are explained by assuming that the human IG-DMR and *RTL1as* have similar functions to the mouse IG-DMR and *Rtl1as*. Indeed, the placental expression data (**Fig. 5a**) are consistent with the deletions and epimutations (hypermethylation) involving the maternally inherited IG-DMR described here, or another yet unidentified IG-DMR(s), resulting in a maternal to paternal epigenotypic alteration with augmented *RTL1* expression. In this case, the excessive *RTL1* expression seems to have a major role in the development of the upd(14)pat-like phenotype, because it is predicted from the mouse data[4,8–10] that cases 3–5, with mild upd(14)pat-like phenotypes, should have moderately increased *RTL1* expression as a result of the presence of a single active copy of *RTL1* in the absence of functional *RTL1as* and that the remaining cases, with typical upd(14)pat phenotypes, should have markedly elevated *RTL1* expression, as in the upd(14)pat cases with two active copies of *RTL1* in the absence of functional *RTL1as* (**Supplementary Table 3**). In support of this, the mouse *Rtl1* is expressed not only in the placenta but also in various fetal tissues including ribs and skeletal muscles[8], and mice with 2.5–3.0 times of *Rtl1* expression caused by maternally derived *Rtl1as* deletion have placental abnormalities[8] similar to those of individuals with the upd(14)pat-like phenotype. By contrast, the typical upd(14)pat phenotype of cases 1 and 2 and the phenotypic similarity between cases 3 and 4 would argue against a

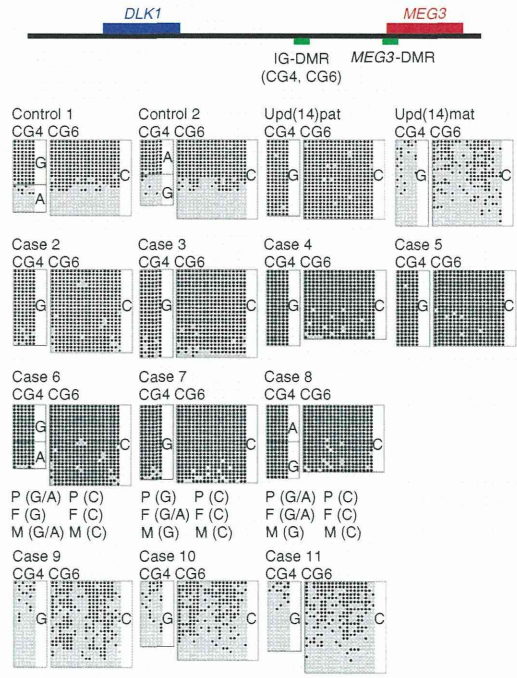

Figure 3 Methylation patterns of the IG-DMR (CG4 and CG6) (those of the *MEG3*-DMR (CG7) are shown in **Supplementary Fig. 2b**). The upper ideogram represents the positions of the IG-DMR and the *MEG3*-DMR. Bisulfite sequencing was done for CG4 and CG6. Each line indicates a single clone, and each circle denotes a CpG island; filled and open circles represent methylated and unmethylated cytosines, respectively. CG4 and CG6 are differentially methylated in control subjects, severely hypermethylated in the upd(14)pat case and cases 2–8 with a upd(14)pat-like phenotype, and grossly hypomethylated in the upd(14)mat case and cases 9–11 with a upd(14)mat-like phenotype. Furthermore, the CG4 SNP typing data (*rs12437020*) are consistent with the parental origin–dependent methylation patterns in the control subjects and show hypermethylation of the maternally derived clones associated with the 'A' allele as well as the paternally derived clones associated with the 'G' allele in case 6 and that of the maternally derived clones associated with the 'G' allele as well as the paternally derived clones associated with the 'A' allele in case 8 (P, patient; F, father; M, mother). The CG6 SNP typing data (*rs10133627*) were not informative. In addition, normal differential methylation patterns were obtained in other examined individuals with a normal phenotype (the father and the maternal grandmother in family A, the father in family B and the parents of cases 4–8) (not shown).

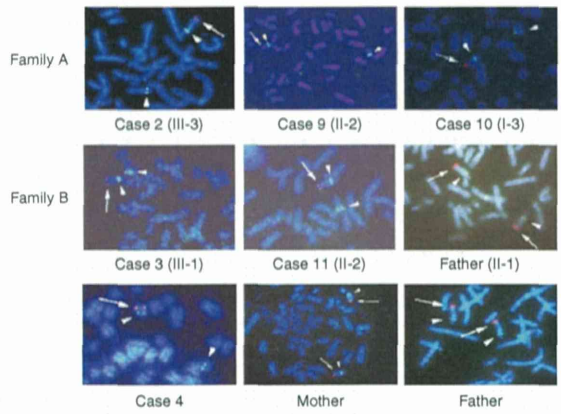

Figure 4 FISH results for the IG-DMR. The red signals (arrows) have been detected by a 5,104-bp LA-PCR product encompassing the CG1–CG6 region (**Fig. 3** and **Supplementary Fig. 2a**), and the green signals (arrowheads) have been identified by an RP11-566I2 probe for 14q12 used as an internal control. Familial heterozygous deletions are identified in cases 2, 9 and 10 of family A and in cases 3 and 11 of family B, and a *de novo* heterozygous deletion is detected in case 4. We also did FISH analyses with a 5,182-bp product encompassing the CG7–CG9 region, showing the same results (not shown).

major role of doubled *DLK1* dosage in the development of upd(14)pat-like phenotype (**Supplementary Table 3**).

The upd(14)mat-like phenotypes of cases 9–11 most likely reflect loss of functional PEGs because it is predicted from the mouse data[4] that deletions involving the paternally derived IG-DMR should not perturb the imprinting status. In this case, loss of active *DLK1* and *RTL1* seems to constitute additive underlying major factors for the development of the upd(14)mat-like phenotype, because a upd(14)mat-like phenotype is common to cases 9–11, who lack active *DLK1*, and growth is more severely compromised in case 11, with additional loss of active *RTL1* (**Supplementary Table 3**). In support of this, the paternally derived *Dlk1* mutation has been previously shown to result in several upd(14)mat-like features, such as pre- and postnatal growth deficiency and obesity and facial abnormalities in mice[22], and the paternally inherited *Rtl1* deletion has been shown to cause mild growth deficiency in mice[8], with the degree of growth failure being ~80% in the two types of knockout mice and ~60% in the MatDi(12) mice lacking functional copies of both *Dlk1* and *Rtl1* (ref. 20). Furthermore, hypomethylation of the paternally inherited DMR adjacent to CG7 has been observed in a single individual with upd(14)mat-like phenotype[23]. This represents a mirror image of epimutations leading to the upd(14)pat-like phenotype and implies that an epimutation is involved in the development of the upd(14)mat-like phenotype.

Although altered *DIO3* and MEGs expression may also be relevant to upd(14)pat/mat phenotypes, the clinical effects would remain minor, if any. Although the primary function of *DIO3* is inactivation of thyroid hormones[24], thyroid dysfunction was absent from cases 1–11 and upd(14)pat/mat cases (this may suggest partial imprinting of human *DIO3*, like that of mouse *Dio3* (ref. 25)) (**Supplementary Tables 1** and **2**). Similarly, although there has been no model mouse with null or doubled MEGs expression that did not show effects on PEGs, *Gtl2*^{lacZ} mice with dysregulated imprinting status caused by a transgene insertion have a normal phenotype with at least 60–80% reduction of all the MEGs[26].

Two findings are noteworthy in reference to the placental studies. First, the methylation profiles of CG4 were similar and those of CG7 were different between leukocytes and placentas of affected and control subjects, as observed in the corresponding regions of normal mice[21]. This implies that the placental imprinting regulation is influenced by the IG-DMR, but is independent of the *MEG3*-DMR, and is also subject to some mechanism(s) such as the control of chromatin conformation[27,28]. Second, phenotypic abnormalities and epigenotypic alterations were identified in the placentas of cases 2 and 8, which had impaired IG-DMRs, whereas they are absent or obscure in the placentas of ΔIG-DMR mice[21]. This suggests that altered gene expression dosage has an essential role in phenotypic development and that there is some difference in IG-DMR function between the human and the mouse placentas (see legend for **Supplementary Fig. 2**).

METHODS

Extraction of DNA and RNA samples. This study was approved by the Institutional Review Board Committee at the National Center for Child Health and Development, and written informed consent was obtained from each subject or his or her parent(s). For leukocytes and fresh placental tissues, we obtained genomic DNA with FlexiGene DNA Kit (Qiagen) and prepared RNA with RNeasy Plus Mini (Qiagen). For paraffin-embedded placental samples, we extracted genomic DNA and RNA with RecoverAll Total Nucleic Acids Isolation Kit (Ambion) using slices of 40 μm thick.

Primers. The primers used in this study are summarized in **Supplementary Table 5** online.

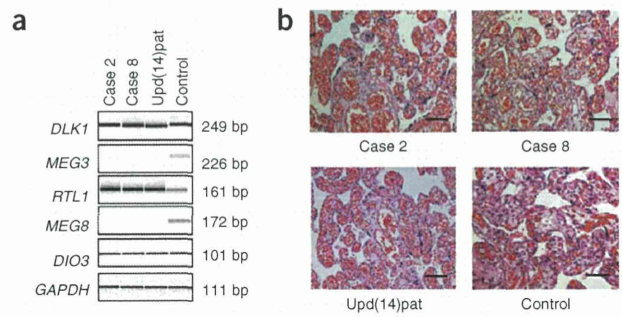

Figure 5 Examinations of placental samples. (**a**) RT-PCR analysis (35–40 cycles) using formalin-treated and paraffin-embedded placental samples of case 2 (30 weeks of gestational age), case 8 (35 weeks), the upd(14)pat case (32 weeks) and a normal subject (33 weeks). *DLK1*, *RTL1* and *DIO3* are expressed and *MEG3* and *MEG8* are not expressed in the placentas of case 2, case 8 and the upd(14)pat case, whereas all the PEGs and MEGs are identified in the control placenta. The results were consistent in RT-PCR experiments performed seven times, except for faint possible *MEG8* expression detected once in the placenta of case 2. Compared to the expression pattern in the control placenta, *RTL1* expression is notably elevated in the placentas of cases 2 and 8 and the upd(14)pat case, and *DLK1* expression is possibly increased in the placentas of case 8 and the upd(14)pat case, although precise quantification was impossible because of poor RNA quality. Although contamination from maternal leukocytes is likely present in these samples, this would not influence the expression pattern, because of absent expression of the imprinted genes in this cell type. (**b**) Histological findings (hematoxylin-eosin staining). The chorionic villi of cases 2 and 8 and the upd(14)pat case are notably proliferated and dilated with congestion, as compared with those of the control subject. The bars represent 100 μm. In addition, nonspecific chorangioma was observed in the placenta of case 2, and interspersed villous calcifications suggestive of degeneration was identified in the placentas of case 8 and the upd(14)pat case.

Genotyping and sequence deletion and variation analyses. Leukocyte genomic DNA was used for these studies. For microsatellite genotyping, we PCR-amplified a segment encompassing each locus with a fluorescently labeled forward primer and an unlabeled reverse primer and determined its size on an ABI PRISM 310 autosequencer using GeneScan software (Applied Biosystems). For polymorphism genotyping, a segment encompassing polymorphism(s) was PCR-amplified and subjected to direct sequencing on a Cequation (8000) autosequencer (Beckman Coulter). For the examination of a tiny deletion and a sequence variation around the *DLK1–MEG3* region, we obtained three LA-PCR products from cases 6–8 and a control subject and subjected them to fragment size comparisons after restriction enzyme digestions and to direct sequencing using serial forward primers (when clear electrochromatograms were not obtained, the corresponding sequences were also analyzed with reverse primers). The three LA-PCR products were a 5,104-bp product encompassing the CG1–CG6 region (also used as FISH probe 1 for the IG-DMR), a 3,142-bp product covering a putative CTCF binding site $(A)^{12}$ and a 5,182-bp product encompassing the CG7–CG9 region and six putative CTCF binding sites $(B–G)^{12}$ (also used as FISH probe 2 for the *MEG3*-DMR). The restriction enzymes used were *Bam*HI, *Kpn*I and *Nco*I for the 5,104-bp product, *Drd*I and *Taq*I for the 3,142-bp product and *Acl*I, *Eco*RI, *Bss*HII, *Kpn*I and *Sac*I for the 5,182-bp product.

Methylation analysis. Leukocyte and placental genomic DNA were treated with bisulfite using the EZ DNA Methylation Kit (Zymo Research) that converts all the cytosines except for methylated cytosines at the CpG islands into uracils and subsequently thymines. We PCR-amplified the CG1–CG9 regions with primer sets that hybridize to both methylated and unmethylated alleles because of absent CpG dinucleotides within the primer sequences. Then, we subcloned the PCR products with the TOPO TA Cloning Kit (Invitrogen) and subjected multiple clones to direct sequencing on the Cequation (8000) autosequencer. When the PCR products contained SNPs, we also carried out genotyping. For CG7, PCR amplification was also done with a methylated allele-specific primer pair hybridizing to a region containing unconverted methylated cytosines and with an unmethylated allele-specific primer pair hybridizing to a region containing thymines converted from unmethylated cytosines, and the PCR products were subjected to gel electrophoresis, as reported previously[5]. For CG8, combined bisulfite restriction analysis (COBRA) was also carried out using a methylated allele-specific *Hga*I restriction site.

FISH analysis. Lymphocyte metaphase spreads were hybridized with probes for specific sequences at the 14q32.2 imprinted region, together with an RP11-566I2 probe for 14q12 used as an internal control. The FISH probes 1 and 2 were as described above, and FISH probes 3 (5,540 bp) and 4 (6,058 bp) were obtained by LA-PCR for the polymorphism-poor sequences at the *DLK1–MEG3* region. We purchased the nine BAC probes covering the imprinted region from BACPAC Resources Center at Children's Hospital Oakland Research Institute. The probes for specific sequences were labeled with digoxigenin and detected by rhodamine anti-digoxigenin, and the control probe was labeled with biotin and detected with avidin conjugated to fluorescein isothiocyanate.

Expression analysis. We analyzed leukocyte and placental RNA for the expression of PEGs and MEGs on the 14q32.2 region. For the imprinted genes other than *RTL1*, cDNA was synthesized from 1 μg of RNA using Superscript III Reverse Transcriptase (Invitrogen), and RT-PCR was done with 20 ng of total RNA using ExTaq (Takara). For *RTL1*, because the primers hybridizing to exon sequences amplify both *RTL1* and *RTL1as*, we used 3′-RACE. We synthesized cDNA from 1 μg of RNA using Superscript III Reverse Transcriptase with a long primer hybridizing to the poly(A) site and introducing the adaptor sequence, and, subsequently, we carried out RT-PCR for 50 ng of cDNA using KOD Dash (Toyobo) with a primer hybridizing to the adaptor sequence and another primer hybridizing to the exon sequence. The reactions were carried out in 200-μl tubes, and small amounts (1–2 μl) of the reaction solutions were loaded onto Gel-Dye Mix (Agilent) after adjusting the *GAPDH* dosage among examined samples.

To examine monoallelic expression in normal placentas, we subjected placental cDNA and genomic DNA and maternal genomic DNA to direct sequencing with primers designed to amplify regions including exonic SNPs (*rs2295660* for *DLK1*; *rs1884540* for *MEG3*; *rs6575805*, *rs11623267*, *rs35695758*, and *rs12884005* for *RTL1*; *rs11847631* and *rs7159526* for *MEG8*; and *rs11627443* and *rs945006* for *DIO3*).

GenBank accession codes. Genome: NC_000014 for *DLK1*, *MEG3*, *RTL1* and *DIO3*, and AL117190 for *MEG8*; mRNA: NM_003836 for *DLK1*, NR_002766 for *MEG3*, XM_370776 for *RTL1*, CA396130 for *MEG8*, and NM_001362 for *DIO3*.

Note: Supplementary information is available on the Nature Genetics website.

ACKNOWLEDGMENTS

We would like to thank all the affected individuals and their family members who participated in this study. This work was supported by Grants for Child Health and Development (17C-2) and for Research on Children and Families (H18-005) from the Ministry of Health, Labor, and Welfare, and by Grants-in-Aid for Scientific Research (priority areas: 16086215 and 1508023; category B: 19390290) from the Ministry of Education, Culture, Sports, Science and Technology.

AUTHOR CONTRIBUTIONS

Molecular analysis was performed by M.K., Y.S., M.I., F.K., M.O. and S.Y., placental sample collection and preparation by H.K., M.N., Y.T., K.M. and K. Ko., placental pathological examination by K.M., and blood sampling and phenotype assessment by G.N., T.T., M.N., Y.T., K.M., T.U., H.K., Y.K., H.O., K. Ku. and T.O. The study was designed and coordinated by F.I. and T.O. with later input from A.C.F.-S., and the results were interpreted and discussed by A.C.F.-S., F.I. and T.O. The paper was written by T.O.

Published online at http://www.nature.com/naturegenetics
Reprints and permissions information is available online at http://npg.nature.com/reprintsandpermissions

1. Cavaille, J., Seitz, H., Paulsen, M., Ferguson-Smith, A.C. & Bachellerie, J.P. Identification of tandemly-repeated C/D snoRNA genes at the imprinted human 14q32 domain reminiscent of those at the Prader-Willi/Angelman syndrome region. *Hum. Mol. Genet.* **11**, 1527–1538 (2002).
2. Charlier, C. *et al.* Human-ovine comparative sequencing of a 250-kb imprinted domain encompassing the callipyge (*clpg*) locus and identification of six imprinted transcripts: *DLK1, DAT, GTL2, PEG11, antiPEG11,* and *MEG8. Genome Res.* **11**, 850–862 (2001).
3. Paulsen, M. *et al.* Comparative sequence analysis of the imprinted *Dlk1-Gtl2* locus in three mammalian species reveals highly conserved genomic elements and refines comparison with the *Igf2–H19* region. *Genome Res.* **11**, 2085–2094 (2001).
4. Lin, S.P. *et al.* Asymmetric regulation of imprinting on the maternal and paternal chromosomes at the *Dlk1-Gtl2* imprinted cluster on mouse chromosome 12. *Nat. Genet.* **35**, 97–102 (2003).
5. Murphy, S.K. *et al.* Epigenetic detection of human chromosome 14 uniparental disomy. *Hum. Mutat.* **22**, 92–97 (2003).
6. Kagami, M. *et al.* Segmental and full paternal isodisomy for chromosome 14 in three patients: narrowing the critical region and implication for the clinical features. *Am. J. Med. Genet. A.* **138**, 127–132 (2005).
7. Kotzot, D. Maternal uniparental disomy 14 dissection of the phenotype with respect to rare autosomal recessively inherited traits, trisomy mosaicism, and genomic imprinting. *Ann. Genet.* **47**, 251–260 (2004).
8. Sekita, Y. *et al.* Role of retrotransposon-derived imprinted gene, *Rtl1*, in the feto-maternal interface of mouse placenta. *Nat. Genet.* advance online publication, doi: 10.1038/ng.2007.51 (6 January 2008).
9. Seitz, H. *et al.* Imprinted microRNA genes transcribed antisense to a reciprocally imprinted retrotransposon-like gene. *Nat. Genet.* **34**, 261–262 (2003).
10. Davis, E. *et al.* RNAi-mediated allelic trans-interaction at the imprinted *Rtl1/Peg11* locus. *Curr. Biol.* **15**, 743–749 (2005).
11. Takahashi, I., Takahashi, T., Utsunomiya, M., Takada, G. & Koizumi, A. Long-acting gonadotropin-releasing hormone analogue treatment for central precocious puberty in maternal uniparental disomy chromosome 14. *Tohoku J. Exp. Med.* **207**, 333–338 (2005).
12. Rosa, A.L. *et al.* Allele-specific methylation of a functional CTCF binding site upstream of *MEG3* in the human imprinted domain of 14q32. *Chromosome Res.* **13**, 809–818 (2005).
13. Kosaki, K. *et al.* Diagnosis of maternal uniparental disomy of chromosome 7 with a methylation specific PCR assay. *J. Med. Genet.* **37**, E19 (2000).
14. Gicquel, C. *et al.* Epimutation of the telomeric imprinting center region on chromosome 11p15 in Silver-Russell syndrome. *Nat. Genet.* **37**, 1003–1007 (2005).
15. Kubota, T. *et al.* Methylation-specific PCR simplifies imprinting analysis. *Nat. Genet.* **16**, 16–17 (1997).
16. Kaneko-Ishino, T., Kohda, T. & Ishino, F. The regulation and biological significance of genomic imprinting in mammals. *J. Biochem.* **133**, 699–711 (2003).

17. Coan, P.M., Burton, G.J. & Ferguson-Smith, A.C. Imprinted genes in the placenta—a review. *Placenta* **26** (Suppl. A), S10–S20 (2005).
18. Kaneko-Ishino, T., Kohda, T., Ono, R. & Ishino, F. Complementation hypothesis: the necessity of a monoallelic gene expression mechanism in mammalian development. *Cytogenet. Genome Res.* **113**, 24–30 (2006).
19. Takada, S. *et al.* Epigenetic analysis of the *Dlk1-Gtl2* imprinted domain on mouse chromosome 12: implications for imprinting control from comparison with *Igf2–H19*. *Hum. Mol. Genet.* **11**, 77–86 (2002).
20. Georgiades, P., Watkins, M., Surani, M.A. & Ferguson-Smith, A.C. Parental origin-specific developmental defects in mice with uniparental disomy for chromosome 12. *Development* **127**, 4719–4728 (2000).
21. Lin, S.P. *et al.* Differential regulation of imprinting in the murine embryo and placenta by the *Dlk1-Dio3* imprinting control region. *Development* **134**, 417–426 (2007).
22. Moon, Y.S. *et al.* Mice lacking paternally expressed Pref-1/Dlk1 display growth retardation and accelerated adiposity. *Mol. Cell. Biol.* **22**, 5585–5592 (2002).
23. Temple, I.K. *et al.* Isolated imprinting mutation of the *DLK1/GTL2* locus associated with a clinical presentation of maternal uniparental disomy of chromosome 14. *J. Med. Genet.* **44**, 637–640 (2007) published online 29 June 2007.
24. Hernandez, A., Martinez, M.E., Fiering, S., Galton, V.A. & St Germain, D.L. Type 3 deiodinase is critical for the maturation and function of the thyroid axis. *J. Clin. Invest.* **116**, 476–484 (2006).
25. Tsai, C.E. *et al.* Genomic imprinting contributes to thyroid hormone metabolism in the mouse embryo. *Curr. Biol.* **12**, 1221–1226 (2002).
26. Sekita, Y. *et al.* Aberrant regulation of imprinted gene expression in *Gtl2*^{lacZ} mice. *Cytogenet. Genome Res.* **113**, 223–229 (2006).
27. Lewis, A. *et al.* Imprinting on distal chromosome 7 in the placenta involves repressive histone methylation independent of DNA methylation. *Nat. Genet.* **36**, 1291–1295 (2004).
28. Umlauf, D. *et al.* Imprinting along the *Kcnq1* domain on mouse chromosome 7 involves repressive histone methylation and recruitment of Polycomb group complexes. *Nat. Genet.* **36**, 1296–1300 (2004).

nature genetics

Role of retrotransposon-derived imprinted gene, *Rtl1*, in the feto-maternal interface of mouse placenta

Yoichi Sekita[1], Hirotaka Wagatsuma[2], Kenji Nakamura[3], Ryuichi Ono[1], Masayo Kagami[4], Noriko Wakisaka[1,5], Toshiaki Hino[3], Rika Suzuki-Migishima[3], Takashi Kohda[1], Atsuo Ogura[6], Tsutomu Ogata[4], Minesuke Yokoyama[3,7], Tomoko Kaneko-Ishino[5] & Fumitoshi Ishino[1]

Eutherian placenta, an organ that emerged in the course of mammalian evolution, provides essential architecture, the so-called feto-maternal interface, for fetal development by exchanging nutrition, gas and waste between fetal and maternal blood. Functional defects of the placenta cause several developmental disorders, such as intrauterine growth retardation in humans and mice. A series of new inventions and/or adaptations must have been necessary to form and maintain eutherian chorioallantoic placenta, which consists of capillary endothelial cells and a surrounding trophoblast cell layer(s)[1]. Although many placental genes have been identified[2], it remains unknown how the feto-maternal interface is formed and maintained during development, and how this novel design evolved. Here we demonstrate that retrotransposon-derived *Rtl1* (retrotransposon-like 1), also known as *Peg11* (paternally expressed 11), is essential for maintenance of the fetal capillaries, and that both its loss and its overproduction cause late-fetal and/or neonatal lethality in mice.

To elucidate *Rtl1* function, we produced knockout (KO) mice (**Supplementary Fig. 1a,b** online). *Rtl1* is a paternally expressed imprinted gene highly expressed at the late-fetal stage in both the fetus and placenta (**Supplementary Fig. 1c**), and it is located in a large imprinted region on distal chromosome 12 (ref. 3; see **Supplementary Table 1** online for imprinting phenotypes[4–6]). Paternally expressed *Rtl1* has an overlapping maternally expressed antisense transcript, *Rtl1* antisense (*Rtl1as*, also known as *antiPeg11*), which contains several microRNAs (miRNAs) targeting the *Rtl1* transcript through an RNAi mechanism[3,7] (**Supplementary Fig. 1a**). We removed the entire Gag- and Pol-like domains of *Rtl1* with approximately 30% homology to the sushi-ichi retrotransposons, together with six of seven miRNAs in *Rtl1as*. Then, we produced two different types of mice: mice with no *Rtl1* expression upon paternal transmission of the KO allele (Pat-KO) and those with 2.5–3.0 times overexpression of the *Rtl1* as a result of deficiency of *Rtl1as* upon maternal transmission (Mat-KO; **Fig. 1a**). We confirmed that the imprinting regulation of distal chromosome 12 was not affected by the KO construct[8,9] (**Supplementary Fig. 1d,e**).

In the course of producing mice with the C57BL/6 (B6) background, we observed that the Pat-KO mice showed pre- and postnatal growth retardation in the F_1 and F_2 generations (**Supplementary Fig. 2a** online), and after the F_3 generation, most showed late-fetal or neonatal lethality (**Fig. 1b,c** and **Supplementary Fig. 3** online). When F_2 males mated with normal B6 females, all the pups, including the wild-type (WT) pups, were born dead as a result of a 3- to 4-d delay of the birth date (**Fig. 1c**; I and II in F_3 generation). When removed by caesarean sections at 19.0 days post coitus (d.p.c.) of the F_3 generation (**Fig. 1c**; III in F_3 generation), the WT pups grew normally, but half of the Pat-KO pups were already resorbing, and the other half were born small (about 80% the weight of the controls) and died by the next day (**Fig. 1c**; III in F_3 generation and **Table 1**). Pat-KO fetuses showed no abnormal phenotypes until 14.5 d.p.c., but half of them died from 15.5 to 19.0 d.p.c. (**Table 1**), and growth retardation of both the fetuses and placentas was observed even in the living half after 15.5 d.p.c. (**Fig. 1d–f**).

In Mat-KO mice, pups, at least after F_2, showed an approximately 15% retardation in growth after weaning (**Supplementary Fig. 2b,c**). Their birth rate gradually diminished after the F_4 generation, and neonatal lethality was predominant in the F_6 generation (**Fig. 1c**, F4–F6; **Supplementary Fig. 3b**, F_4–F_6 and **Supplementary Table 2** online). All the Mat-KO pups reached term normally, with normal weight, but they showed 150% placentomegaly compared to the normal size, and most died within a day (**Fig. 1g,h**). Although the genetic background affected both the Pat-KO and Mat-KO phenotypes to a large degree (**Supplementary Tables 2** and **3** online), these results demonstrate that both the loss and the overproduction

[1]Department of Epigenetics, Medical Research Institute, Tokyo Medical and Dental University, 2-3-10 Kandasurugadai, Chiyoda-ku, Tokyo 101-0062, Japan. [2]Graduate School of Bioscience and Biotechnology, Tokyo Institute of Technology, 4259 Nagatsuta-cho, Midori-ku, Yokohama 226-8501, Japan. [3]Mitsubishi Kagaku Institute of Life Sciences, 11 Minamiooya, Machida, Tokyo 194-8511, Japan. [4]Department of Endocrinology and Metabolism, National Research Institute for Child Health and Development, 2-10-1 Okura, Setagaya-ku, Tokyo 157-8535, Japan. [5]School of Health Sciences, Tokai University, Bohseidai, Isehara, Kanagawa 259-1193, Japan. [6]BioResource Center, RIKEN, 3-1-1 Koyadai, Tsukuba, Ibaraki 305-0074, Japan. [7]Present address: Brain Research Institute, Niigata University, 1-757 Asahimachi-dori, Niigata 951-8585, Japan. Correspondence should be addressed to T.K.-I. (tkanekoi@is.icc.u-tokai.ac.jp) or F.I. (fishino.epgn@mri.tmd.ac.jp).

Received 21 May 2007; accepted 16 October 2007; published online 6 January 2008; doi:10.1038/ng.2007.51

of *Rtl1* interfered with normal fetal development, providing direct evidence for the importance of both retrotransposon-derived *Rtl1* and microRNAs in *Rtl1as*.

Histological analyses demonstrated that severe abnormalities occur in the same place in both the Pat-KO and Mat-KO placentas (that is, the fetal capillaries where the feto-maternal interaction occurs), but the consequences of these abnormalities were different (**Fig. 2**). The mouse placenta consists of three major zones: the decidua basalis, the junctional zone and the labyrinth zone. In the Pat-KO placenta at 15.5 d.p.c., we found abnormal, dark-stained regions in the labyrinth zone upon hematoxylin and eosin (HE) staining (**Fig. 2a**, WT; **b,c**, Pat-KO). Using truidin blue staining and electron microscopy, we confirmed several morphological abnormalities throughout the labyrinth zone, such as splitting of the basement membrane (**Fig. 2d,h**, WT; **e,i**, Pat-KO), the emergence of a number of lysosomes in layer III trophoblast cells (**Fig. 2f,j**) and clogging in the fetal capillaries (**Fig. 2g,k**). When we did immunohistochemical (IHC) staining with CD31, an endothelial cell–specific marker, we observed that its

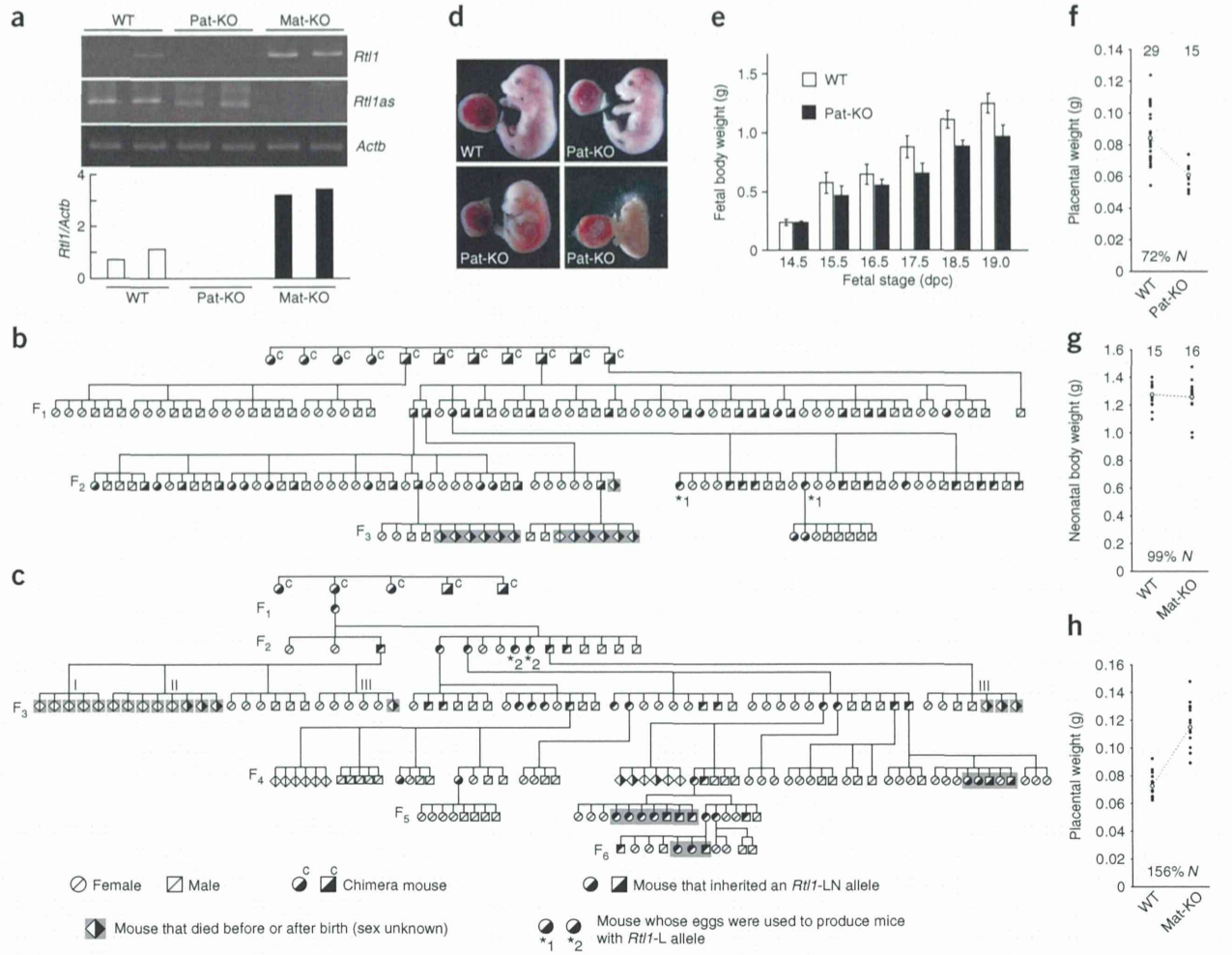

Figure 1 Pedigree of *Rtl1* KO mice. (**a**) Expression of *Rtl1* and *Rtl1as* in WT, Pat-KO and Mat-KO fetuses (*Rtl1*-LN) as determined by RT-PCR. β-actin (encoded by *Actb*) used as a control. The band intensities, measured using ImageJ software are shown below. (**b**) A pedigree from a male chimera. (**c**) A pedigree from a female chimera. A 4-d delay of natural delivery (I) and a caesarean section after a 3-d delay from the expected delivery date (II). All pups were dead in both cases. Caesarean sections were carried out at 19.0 d.p.c. when paternal transmission was analyzed (III). From the F_1 males and females, we obtained many Pat-KO and Mat-KO mice, although the number of Pat-KO mice was slightly smaller than expected from the mendelian ratio (WT/Pat-KO = 24:19, **Supplementary Table 1**) and they grew to adulthood with a reduced body weight (**Supplementary Fig. 2**). Thus, it is clear that the F_1 males and females with the C57BL/6 × 129/Sv F1 (B6/129) genetic background from chimera mice can produce some viable Pat-KO and Mat-KO pups. (**d**) Fetuses at 16.5 d.p.c, including a WT fetus (upper left) and Pat-KO fetuses: small normal-looking (alive) fetus (upper right), pale dead fetus (lower left), and resorbing fetus (lower right). Scale bar, 10 mm. (**e**) Late-fetal growth retardation in Pat-KO fetuses. Open bars, WT fetal body weight; solid bars, Pat-KO fetal body weight. (**f–h**) Growth phenotype of Pat-KO placentas at 18.5 d.p.c. (**f**) and Mat-KO neonates (**g**) and Mat-KO placentas (**h**) at birth (caesarean section). The data in **g** and **h** are from the same litters. Each filled circle represents a single placenta and neonate, respectively. The number at the top represents the total number of weighted samples. Open circles represent average weight. The degree of growth deficiency or promotion of mutant mice is shown as the percentage of WT weight (*N*). Placental and neonatal body weights (mean ± s.d.) are as follows: **f**; WT, 0.085 ± 0.015 ($n = 29$); Pat-KO, 0.061 ± 0.008 ($n = 15$); $P = 1.805 \times 10^{-65}$ (*t*-test), **g**; WT, 1.279 ± 0.087 ($n = 15$); Mat-KO, 1.262 ± 0.126 ($n = 16$), **h**; WT, 0.073 ± 0.009 ($n = 15$); Mat-KO, 0.116 ± 0.016 ($n = 16$); $P = 9.721 \times 10^{-105}$ (*t*-test).

Table 1 Lethality of *Rtl1*-LN (Pat-KO) fetuses and neonates at F_3

Dissection stage (d.p.c.)	WT total	Pat-KO total (dead)	Percentage death in Pat-KO
12.5	5	4 (0)	0
14.5	5	5 (0)	0
15.5	9	7 (1)	14.3
16.5	9	11 (5)	45.5
17.5	10	11 (6)	54.5
18.5	21	24 (13)	54.2
Neonate	35	13 (13)	100

signal diffused to the area of the trophoblast cells (**Fig. 2l**, WT; **m,n**, Pat-KO). These results indicate that a phagocytic reaction to the endothelial cells was induced in the surrounding layer III trophoblast cells. Thus, the resulting placental infarction seems to cause placental malfunction, such as incomplete material transport between the maternal and the fetal blood, presumably leading to the late-fetal growth retardation and lethality in the Pat-KO fetuses.

We confirmed functional deficiency of the Pat-KO placenta by nutrition transfer assay[10,11]. We examined both active and passive transport at 15.5 d.p.c. using two radiolabeled substrates, [^{14}C]methylaminoisobutyric acid (Me-AIB) and [^{14}C]inulin, respectively. We did not find any significant difference between WT and Pat-KO placentas in materno-fetal transfer of [^{14}C]Me-AIB, a non-metabolizable amino acid analog, through the System A amino acid transport system ($P = 0.158$; **Fig. 3a**). However, the passive permeability of inulin was significantly lower in Pat-KO placenta (48% compared with WT, $P = 0.000123$; **Fig. 3b**), indicating that Rtl1 deficiency had damaged the placental physical barrier but had not affected the active transport system[12]. In the case of Mat-KO, placentomegaly was associated with expansion of the inner spaces of the fetal capillaries (**Fig. 1h** and **Fig. 2o**, WT; **p**, Mat-KO, and **q**). The most severe abnormalities were found in the surrounding layer III trophoblast cells, which showed a large number of vacuoles, indicating that these cells were starving (**Fig. 2r**, WT; **s,t**, Mat-KO).

IHC staining with antibody to Rtl1 showed that Rtl1 protein localized exclusively in the labyrinth zone at 18.5 d.p.c.; no signals in the other layers of the placenta were observed (**Fig. 4a–d**). Co-immunostaining with CD31 showed that Rtl1 localized around the nuclei of the capillary endothelial cells, where anomalies in both Pat-KO and Mat-KO were observed (**Fig. 4e**). We did not observe any signals in the Pat-KO placentas, but we observed strong signals in the

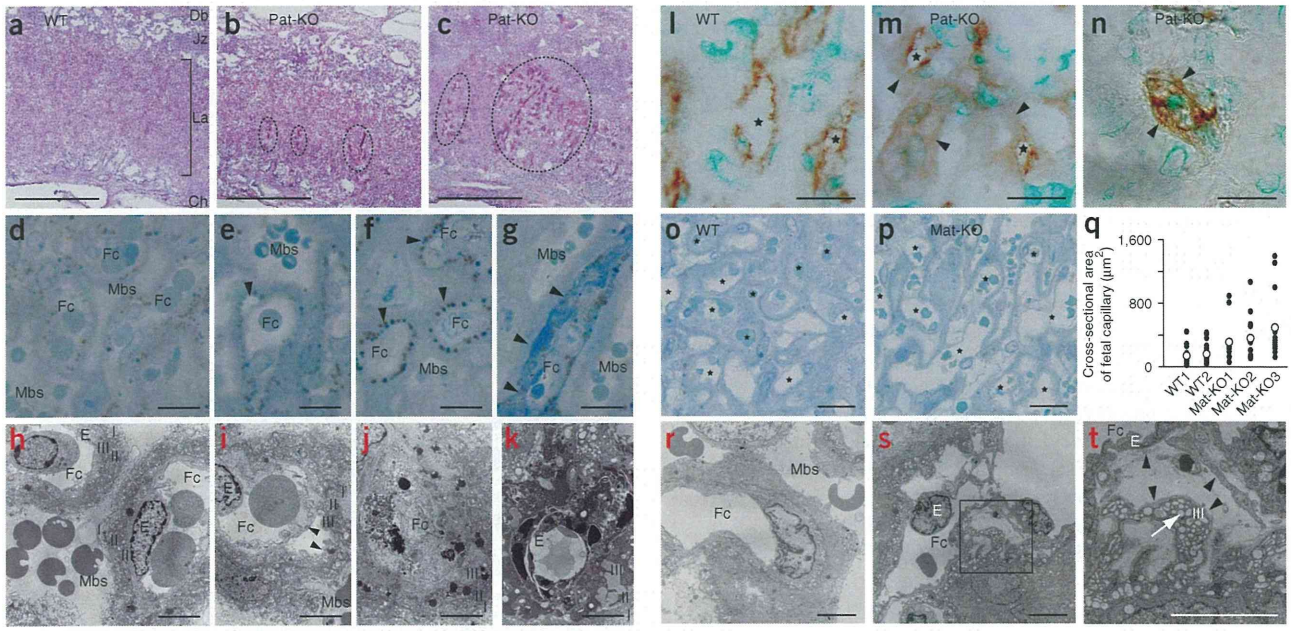

Figure 2 Histological abnormalities observed in day 15.5 Pat-KO placentas and in day 18.5 Mat-KO placentas. Most abnormalities were observed near the endothelial cells and the surrounding layer III trophoblast of the fetal capillaries in the labyrinth zone. (**a–n**) The labyrinth zone of WT placentas at 15.5 d.p.c. is shown in **a**, **d**, **h** and **l** and that of Pat-KO placentas at the same stage is shown in **b**, **c**, **e–g**, **i–k**, **m** and **n**. (**o–s**) The labyrinth zone of WT placenta at 18.5 d.p.c. is shown in **o** and **r**, and that of the Mat-KO placenta at the same stage is shown in **p** and **s**. H&E staining in **a–c**; scale bar, 0.5 mm. Truidin blue staining in **d–g**,**o** and **p**; scale bar, 10 μm for **d–g**, 20 μm for **o** and **p**. The arrowheads indicate an abnormal space between the endothelial cell and the layer III trophoblast in **e**, abnormally appearing lysosomes in **f** and a clogged fetal capillary in **g**. Clogging, as seen in **g** and **k**, was found mainly in the dark-stained regions, as shown in the dotted circles in **b** and **c**. Electron microscopy images in **h–k**,**r** and **s**; scale bar, 5 μm. The arrowheads indicate an abnormal space between the endothelial cell and the layer III trophoblast in **i**. (**t**) Magnified figure of the square area in **s**; scale bar, 5 μm. The black arrowheads indicate an abnormal space between the endothelial cell and the layer III trophoblast, and the white arrow indicates vacuoles in the layer III trophoblast. IHC staining in **l–n** with antibody to CD31; scale bar, 20 μm. The arrowheads indicate an abnormally diffused signal of endothelial cell marker in **m** and a disrupted fetal capillary in **n**. The same result was obtained with an antibody to CD34, another endothelial specific marker (data not shown). **q** shows a cross-sectional area of fetal capillary that was measured using ImageJ. The Pat-KO fetus associated with placenta **c** and **n** was already dead at 15.5 d.p.c. At present, it remains unclear whether the neonatal lethal phenotypes in both Pat-KO and Mat-KO are primarily due to direct or indirect effects of the severe placental anomalies, although both are likely to be involved. Further investigation will be necessary to reveal whether there is a specific cause for neonatal lethality. Db, decidua basalis; Jz, junctional zone; Lz, labyrinth zone; Ch, chorionic plate; Mbs, maternal blood sinus; Fc, fetal capillary; E, endothelial cell; I/II/III, layer I/II/III trophoblast. The asterisks in **l–p** indicate fetal capillaries.

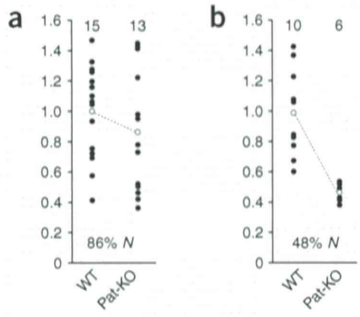

Figure 3 Placental transfer assay. (**a**) Placental transfer of [^{14}C]Me-AIB at 15.5 d.p.c. (**b**) Placental transfer of [^{14}C]inulin at 15.5 d.p.c. Each substrate was injected from the jugular vein of pregnant females at 15.5 d.p.c., and the amount of the labeled substances that entered the fetus through the placenta was determined 3–4 min after injection[10,11]. The fetal accumulation of radioisotope per milligram of placenta was calculated and compared between WT and Pat-KO. The average of WT in every littermate was defined as 1. No significant difference in the active transfer of Me-AIB between WT and Pat-KO placenta was found (86%, $P = 0.158$). However, the passive permeability of inulin in Pat-KO was decreased to about 50% of that in WT (48%, $P = 0.000123$).

Mat-KO placentas, as expected (**Fig. 4f,g**; see also **Supplementary Fig. 4** online). No Rtl1 protein was detected in the endothelial cells of the umbilical cord, although they are connected to the fetal capillaries and are of the same origin as placental endothelial cells (**Fig. 4a,d**). Therefore, we concluded that Rtl1 functions exclusively in the placental endothelial cells for the maintenance of the feto-maternal interface during late-fetal development. To create the novel feto-maternal interface in the course of evolution, the endothelial cells may need a unique protein to regulate the trophoblast cells that have intrinsically invasive and phagocytotic features.

These experiments demonstrate that among several candidate imprinted genes, *Rtl1* is one of the major genes responsible for maternal and paternal duplication of distal chromosome 12 (PatDp (dist12) and MatDp(dist12)) as well as for the corresponding uniparental disomies (MatDi(12) and PatDi(12))[4–6] (**Supplementary Table 1**). The MatDp(dist12) phenotypes of late-fetal and neonatal lethality associated with intrauterine growth retardation are consistent with those of *Rtl1* Pat-KO. *Dlk1* Pat-KO and *Dio3* null mice also showed reduced neonatal size and viability to a certain degree, but this did not account for the severe lethality of MatDp(dist12) and MatDi(12)[13,14]. Therefore, we conclude that the loss of *Rtl1* expression has an important role in such late-fetal viability and that *Dlk1, Rtl1* and possibly *Dio3* can independently contribute to late-fetal growth and neonatal lethality. *Rtl1* Mat-KO mice show notable overgrowth and morphological abnormalities of the placenta consistent with the PatDi(12) mice phenotypes[15]. The Mat-KO mice show only a 2.5- to 3.0-fold increment of *Rtl1* from a single normal paternal allele as a result of the lack of *Rtl1as* from the maternal allele. Therefore, an approximately 4.5-fold overexpression of *Rtl1* from the two paternal alleles that would be expected in PatDi(12) and PatDp(dist12) mice[9] may explain their late-fetal lethality, rather than the neonatal lethality in the Mat-KO.

Rtl1 is one of 11 retrotransposon-derived genes related to the sushi-ichi retrotransposon that are specifically conserved in eutherian mammals[16–20]. Eutherian orthologs of *Rtl1* have a high degree of amino acid conservation and low synonymous-to-nonsynonymous substitution rates (dN/dS), supporting the claim that *Rtl1* has a common and crucially important function in the placenta among eutherians, including human beings[17,21] (**Supplementary Fig. 5** online). This work provides evidence for exaptation, the acquisition

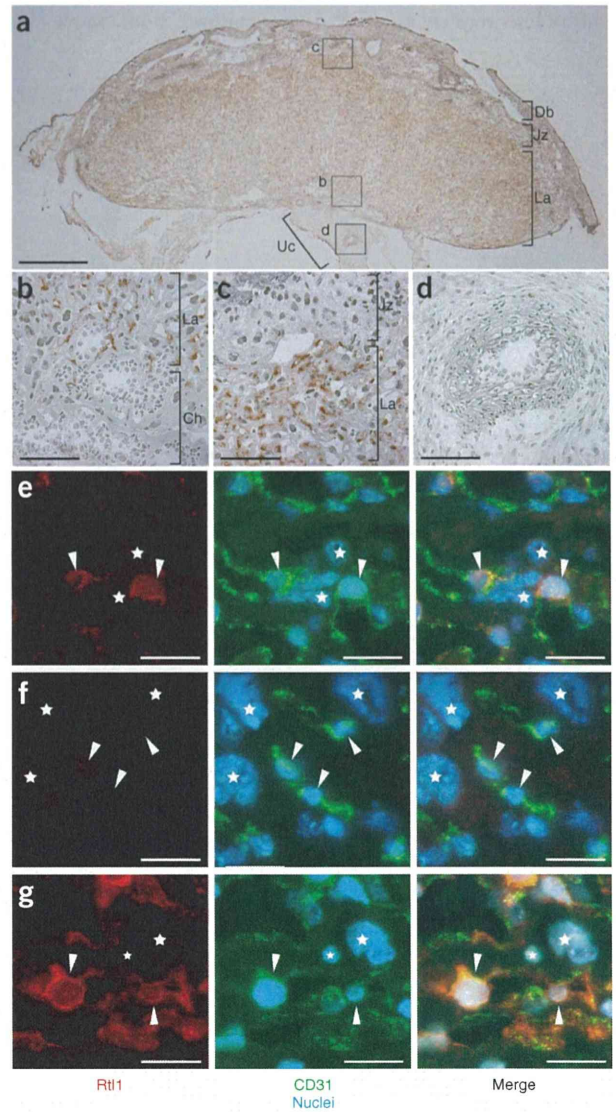

Figure 4 Rtl1 protein localization in the placentas at 18.5 d.p.c. by immunohistochemistry. (**a–c**) Whole placenta image (**a**) and its magnified images (indicated as each small square) of the boundary regions of the placental zones between the labyrinth zone (La) and chorionic plate (Ch) (**b**) and between La and the junctional zone (Jz) (**c**). (**d**) Umbilical cord (Uc) connecting to the fetal capillaries. The signals of Rtl1 (brown by DAB staining) are seen exclusively in La but not in Ch, Jz, decidual basalis (Db) or Uc. Scale bar, 1 mm for **a** and 100 μm for **b–d**. (**e–g**) Co-immunostaining of Rtl1 (red, left), CD31 and nuclei (green and blue, respectively, middle) and their merged image (right). The labyrinth zones of WT (**e**), Pat-KO (**f**) and Mat-KO (**g**) are shown. The arrowheads and stars indicate nuclei of endothelial cells and trophoblast cells, respectively. Scale bar, 20 μm. Only the perinuclear region in the endothelial cells were stained by antibody to Rtl1 in WT (**e**) and Mat-KO (**g**). Note that the inner areas of the endothelial cells were also stained when Rtl1 was overproduced in Mat-KO (**g**; left and right).

of new genomic function from transposons[22–29]. We have recently shown that *Peg10* is also essential for placenta formation[18]. Although both *Rtl1* and *Peg10* are derived from the sushi-ichi–related retrotransposon, they have divergent roles, as expected from their amino acid sequences and as shown by the results of knockout experiments. *Peg10* has a DNA/RNA binding motif and an aspartyl protease motif, and it functions in placenta formation, especially in the trophoblast lineage, at an early embryonic stage. *Rtl1*, however, has only an aspartyl protease motif and functions in the maintenance of the feto-maternal interface at the late-fetal stage[16]. The important implication of these findings is that two independent exaptation events of the sushi-ichi–related retrotransposons have contributed to two different steps of placental development in the mouse.

In this work, we demonstrate that the retrotransposon-derived gene *Rtl1* is a key gene in placental development and evolution and is one of the primary genes responsible for phenotypic development in mouse PatDp(dist12)/MatDp(dist12) as well as PatDi(12)/MatDi(12). Because the remaining nine retrotransposon-derived genes also possess putative proteins, and at least some of them show expression in the placenta[16–20], identification of their origins and functions may provide important insight into placental evolution.

METHODS

Deletion of the *Rtl1* gene. Experimental procedures in this work were approved by the Animal Ethics Committees of Tokyo Medical and Dental University. We obtained 1.8-kb (nucleotides 67,582,103–67,580,338) and 7.3-kb (nucleotides 67,586,373–67,593,715) genomic DNA fragments from a mouse BAC (mRG158M19) clone containing the *Rtl1* ORF (nucleotides 67,581,614–67,586,845) and used them as the right- and left-arm sequences of a construct in which the *Rtl1* ORF was replaced with the neomycin-resistance gene. The nucleotide numbers refer to the sequence with accession number NT_039551.6. After a 2-week incubation under G418 selection, followed by electroporation of the linearized DNA into embryonic stem cells (CCE) of 129/SvEv mouse origin, we obtained 120 colonies. The genomic DNA was checked using DNA blot analysis with DNA fragments of nucleotides 67,580,998–67,581,906 and 67,607,241–67,608,065 as the 5′ and 3′ probes, respectively.

Using the *Rtl1*-targeted embryonic stem cells resulting from the homologous recombination of the construct, we made chimeric mice by blastocyst injection. Germline transmission of the knockout allele was confirmed in one male and one female chimera (*Rtl1*-LN). We carried out *in vitro* fertilization using normal C57BL/6 sperm and eggs from two *Rtl1*-LN females (indicated by the asterisks 1 and 2 in **Figure 1b** and **c**, respectively) and injected the *Cre* recombinase expression vector (pCAGGS-Cre) into the resulting fertilized eggs to produce mice that had *Rtl1*-L alleles.

All of the *Rtl1* KO lines were maintained by continuous crossing with WT B6 males and females to the F_8 generation, unless otherwise indicated.

Expression analyses of imprinted genes. Genomic DNA and total RNA were prepared from day 14.5 fetuses using ISOGEN (Nippon Gene). The methods for the quantitative RT-PCR for *Dlk1*, *Dio3*, *Meg3/Gtl2*, *Meg8/Rian* and 3′-RACE for *Rtl1* and *Rtl1as* followed by cDNA synthesis have been described previously[30]. The band intensity of *Rtl1* was measured using ImageJ software (see URLs section below).

DNA methylation analyses of IG-DMR and *Gtl2*-DMR. Purified genomic DNA was treated with sodium bisulfite solution, and the resulting DNA was amplified by the primers described previously[30]. We used the combined bisulfite restriction analysis (COBRA) method with the restriction enzyme *AciI* for IG-DMR and *TaqI* for *Gtl2*-DMR.

Placenta functional assay. We examined the efficiencies of nutrition transfer through the placenta at 15.5 d.p.c. in every fetus and placenta of the two to three litters using two radiolabeled substrates, [^{14}C]Me-AIB and [^{14}C]inulin, to measure the active and passive transport, respectively[10,11]. These substrates were dissolved in PBS and injected into the jugular vein of pregnant females. Three to four minutes after injection, the females were dissected and fetuses and placentas were sampled, because it is reported that there is minimal backflux of the radioisotopes from fetus to mother for up to 5 min[11]. The amount of the labeled substance in the fetuses and placentas was determined by a liquid scintillation counter. The counts of fetuses per milligram of placentas were calculated as the placental transfer efficiency, and the average of WT fetuses in each litter was set as 1. We compared WT and Pat-KO. Materno-fetal transfer of Me-AIB, a non-metabolizable amino acid analog usually transported across the placenta, reflects the activity of the System A amino acid transport system, whereas that of inulin reflects the passive permeability that is usually affected by the exchange barrier surface area, thickness and fetal blood flow. Using this assay, we detected only background levels of radioisotopes in the dead fetuses, whereas we found that the levels in their placentas were almost the same as that of WT and living Pat-KO placentas, providing evidence that the maternal blood flow in the placentas was still normal, even in the dead fetuses.

Histological analyses. The placentas for hematoxylin and eosin staining and IHC staining were collected and embedded in OCT compound immediately. Then, 5-μm sections were made. For hematoxylin and eosin staining, we fixed the sections in 4% paraformaldehyde (PFA) before performing the standard staining procedure. The sections were fixed in acetone for the immunostaining of CD31 and CD34, or 4% PFA for the immunostaining of Rtl1. Antibody to CD31 and antibody to CD34 (BD Pharmingen) were each used as the primary antibody, and then horseradish peroxidase (HRP)-labeled anti-rat IgG (Jackson ImmunoResearch Laboratories) was added as the secondary antibody. The antibody to Rtl1 that was produced from rabbit serum by immunizing with the synthetic Rtl1 peptide (NH_2-CGDQEAVTFRPRN-COOH) was used as the primary antibody, and then HRP-labeled anti-rabbit IgG (GE Healthcare Bio-Sciences) was added as the secondary antibody. HRP activities were visualized by diaminobenzidine (DAB) staining, and the nuclei were stained using 2% methyl green. For co-immunostaining of Rtl1 and CD31, the sections were fixed in 4% PFA. The primary antibody mixture including the antibody to CD31 and the antibody to Rtl1, and the secondary antibody mixture including the Alexa 488-conjugated anti-rat IgG (Invitrogen), Cy3-conjugated anti-rabbit IgG (Jackson ImmunoResearch Laboratories) and Hoechst 33342, were used. Images were captured and overlaid by a VB-7000 Digital Camera System (Keyence). For truidin blue staining and transmission electron microscopy, we fixed the placentas in 2.5% glutaraldehyde in 0.05 M PBS and 1% osmium tetroxide before following the standard staining methodology.

URLs. ImageJ software, http://rsb.info.nih.gov/ij/.

GenBank accession codes. The nucleotide numbers refer to the sequence of mouse chromosome 12 with accession number NT_039551.6.

Note: Supplementary information is available on the Nature Genetics website.

ACKNOWLEDGMENTS

We thank S. Aizawa of Center for Developmental Biology, RIKEN for providing the DT-A vector that was used for making *Rtl1* KO construct, E. Robertson of University of Oxford for the CCE ES cells, M. Constancia of University of Cambridge for placenta functional assay protocol, Y. Nakahara and M. Takabe of the Mitsubishi Kagaku Institute of Life Sciences for animal breeding and H. Hasegawa, N. Kawabe and A. Akatsuka of the Tokai University and S. Ichinose of the Tokyo Medical and Dental University for their assistance in immunohistochemistry and electron microscopy along with helpful discussion. This work was supported by grants from Creative Science Research, the research program of Japan Society for the Promotion of Science (JSPS), the Uehara Memorial Science Foundation, the Mitsubishi Foundation and the Ministry of Health, Labour and Welfare for Child Health and Development (17C-2) and a Grant-in-Aid for Scientific Research on Priority Areas form the Ministry of Education, Culture, Sports, Science and Technology of Japan (1508023) to F.I., the grant for young investigators from Medical Research Institute to Y.S., and the Asahi Glass Foundation and JSPS, Grants-in Aid for Scientific Research to T.K.-I. Pacific Edit reviewed the manuscript before submission.

AUTHOR CONTRIBUTIONS

Most analyses in this work were performed by Y.S. with collaboration of H.W., R.O., N.W., T.K. and M.K. in molecular and histological experiments.

Construction of *Rtl1* targeting vector was done by H.W. under supervision of K.N. and M.Y., and KO mice were produced by T.H., R.S.-M., K.N. and M.Y. The study was designed and coordinated by T.K.-I. and F.I., and the results were discussed by A.O., T.O., T.K.-I. and F.I. The paper was written by Y.S. and F.I.

Published online at http://www.nature.com/naturegenetics
Reprints and permissions information is available online at http://npg.nature.com/reprintsandpermissions

1. Rossant, J. & Cross, J.C. Placental development: lessons from mouse mutants. *Nat. Rev. Genet.* **2**, 538–548 (2001).
2. Watson, E.D. & Cross, J.C. Development of structures and transport functions in the mouse placenta. *Physiology (Bethesda)* **20**, 180–193 (2005).
3. Seitz, H. *et al.* Imprinted microRNA genes transcribed antisense to a reciprocally imprinted retrotransposon-like gene. *Nat. Genet.* **34**, 261–262 (2003).
4. Cattanach, B.M. & Rasverry, C.V. Evidence of imprinting involving the distal region of Chr 12. *Mouse Genome* **91**, 858 (1993).
5. Georgiades, P., Watkins, M., Surani, M.A. & Ferguson-Smith, A.C. Parental origin-specific developmental defects in mice with uniparental disomy for chromosome 12. *Development* **127**, 4719–4728 (2000).
6. Tevendale, M., Watkins, M., Rasberry, C., Cattanach, B. & Ferguson-Smith, A.C. Analysis of mouse conceptuses with uniparental duplication/deficiency for distal chromosome 12: comparison with chromosome 12 uniparental disomy and implications for genomic imprinting. *Cytogenet. Genome Res.* **113**, 215–222 (2006).
7. Davis, E. *et al.* RNAi-mediated allelic trans-interaction at the imprinted *Rtl1/Peg11* locus. *Curr. Biol.* **15**, 743–749 (2005).
8. Takada, S. *et al.* Epigenetic analysis of the *Dlk1-Gtl2* imprinted domain on mouse chromosome 12: implications for imprinting control from comparison with *Igf2-H19*. *Hum. Mol. Genet.* **11**, 77–86 (2002).
9. Lin, S.P. *et al.* Asymmetric regulation of imprinting on the maternal and paternal chromosomes at the *Dlk1-Gtl2* imprinted cluster on mouse chromosome 12. *Nat. Genet.* **35**, 97–102 (2003).
10. Constância, M. *et al.* Placental-specific IGF-II is a major modulator of placental and fetal growth. *Nature* **417**, 945–948 (2002).
11. Sibley, C.P. *et al.* Placental-specific insulin-like growth factor 2 (*Igf2*) regulates the diffusional exchange characteristics of the mouse placenta. *Proc. Natl. Acad. Sci. USA* **101**, 8204–8208 (2004).
12. Angiolini, E. *et al.* Regulation of placental efficiency for nutrient transport by imprinted genes. *Placenta* **27** (Suppl. A), S98–S102 (2006).
13. Moon, Y.S. *et al.* Mice lacking paternally expressed Pref-1/Dlk1 display growth retardation and accelerated adiposity. *Mol. Cell. Biol.* **22**, 5585–5592 (2002).
14. Hernandez, A., Martinez, M.E., Fiering, S., Galton, V.A. & St Germain, D. Type 3 deiodinase is critical for the maturation and function of the thyroid axis. *J. Clin. Invest.* **116**, 476–484 (2006).
15. Georgiades, P., Watkins, M., Burton, G.J. & Ferguson-Smith, A.C. Roles for genomic imprinting and the zygotic genome in placental development. *Proc. Natl. Acad. Sci. USA* **98**, 4522–4527 (2001).
16. Butler, M., Goodwin, T., Simpson, M., Singh, M. & Poulter, R. Vertebrate LTR retrotransposons of the Tf1/sushi group. *J. Mol. Evol.* **52**, 260–274 (2001).
17. Lynch, C. & Tristem, M. A co-opted gypsy-type LTR-retrotransposon is conserved in the genomes of humans, sheep, mice, and rats. *Curr. Biol.* **13**, 1518–1523 (2003).
18. Ono, R. *et al.* Deletion of *Peg10*, an imprinted gene acquired from a retrotransposon, causes early embryonic lethality. *Nat. Genet.* **38**, 101–106 (2006).
19. Brandt, J. *et al.* Transposable elements as a source of genetic innovation: expression and evolution of a family of retrotransposon-derived neogenes in mammals. *Gene* **345**, 101–111 (2005).
20. Youngson, N.A., Kocialkowski, S., Peel, N. & Ferguson-Smith, A.C. A small family of sushi-class retrotransposon-derived genes in mammals and their relation to genomic imprinting. *J. Mol. Evol.* **61**, 481–490 (2005).
21. Kagami, M. *et al.* Deletions and epimutations affecting the human 14q32.2 imprinted region in individuals with paternal and maternal upd(14)-like phenotypes. *Nat. Genet.* advance online publication, doi:10.1038/ng.2007.56 (6 January 2008).
22. Gould, S. & Vrba, S. Exaptation—a missing term in the science of form. *Paleobiology* **8**, 4–15 (1982).
23. Brosius, J. & Gould, S.J. On "genomenclature": a comprehensive (and respectful) taxonomy for pseudogenes and other "junk DNA". *Proc. Natl. Acad. Sci. USA* **89**, 10706–10710 (1992).
24. Smit, A.F. Interspersed repeats and other mementos of transposable elements in mammalian genomes. *Curr. Opin. Genet. Dev.* **9**, 657–663 (1999).
25. Mi, S. *et al.* Syncytin is a captive retroviral envelope protein involved in human placental morphogenesis. *Nature* **403**, 785–789 (2000).
26. Kazazian, H.H., Jr. Mobile elements: drivers of genome evolution. *Science* **303**, 1626–1632 (2004).
27. Dupressoir, A. *et al.* Syncytin-A and syncytin-B, two fusogenic placenta-specific murine envelope genes of retroviral origin conserved in Muridae. *Proc. Natl. Acad. Sci. USA* **102**, 725–730 (2005).
28. Bejerano, G. *et al.* A distal enhancer and an ultraconserved exon are derived from a novel retroposon. *Nature* **441**, 87–90 (2006).
29. Biémont, C. & Vieira, C. Genetics: junk DNA as an evolutionary force. *Nature* **443**, 521–524 (2006).
30. Sekita, Y. *et al.* Aberrant regulation of imprinted gene expression in *Gtl2*^{lacZ} mice. *Cytogenet. Genome Res.* **113**, 223–229 (2006).